



Supplement of

Contribution of physical latent knowledge to the emulation of an atmospheric physics model: a study based on the LMDZ Atmospheric General Circulation Model

Sékolène Crossouard et al.

Correspondence to: Sékolène Crossouard (segolene.crossouard@lsce.ipsl.fr)

The copyright of individual parts of the supplement might differ from the article licence.

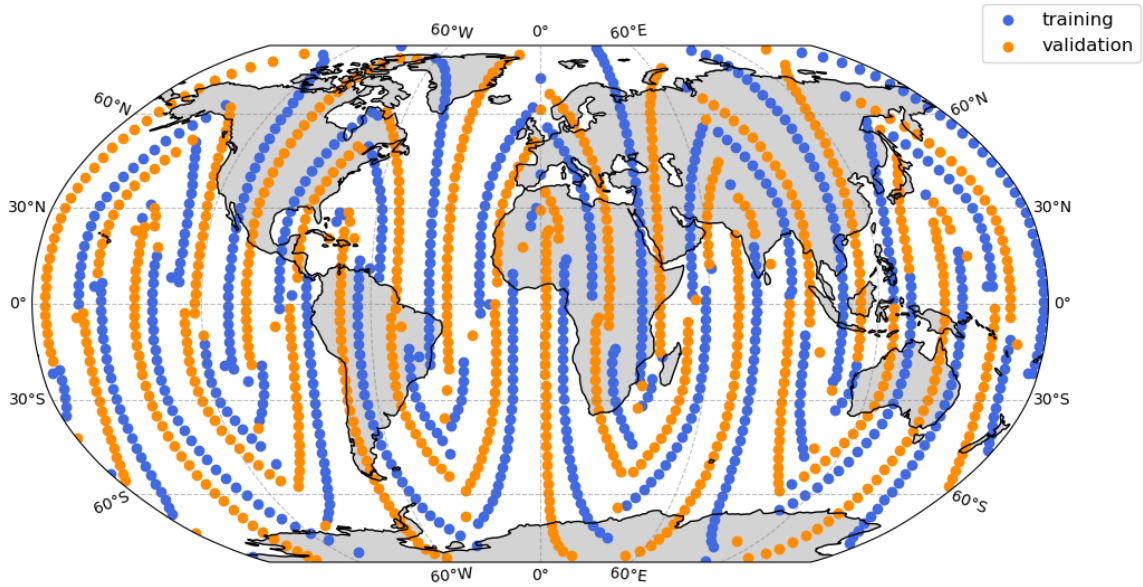


Figure S1. Distribution of grid cells over the globe used for training in blue and validation in orange, for the realistic configuration. The same distribution of grid cells is used for the aquaplanet.

Table S1. Description of the DNN architecture used for the first learning—the initial training without laplacian—and the second learning—with laplacians as additional predictors.

Step	Layer	Number of neurons	Number of parameters 1 st learning	Number of parameters 2 nd learning
Input	Input	X' length	0	0
Hidden layers	Dense	512	285,184	527,872
	Dense	512	262,656	262,656
	Dense	512	262,656	262,656
	Dense	512	262,656	262,656
	Dense	512	262,656	262,656
	Dense	512	262,656	262,656
Output	Dense	Y' length	243,162	243,162
Total number of parameters			1,841,626	2,084,314

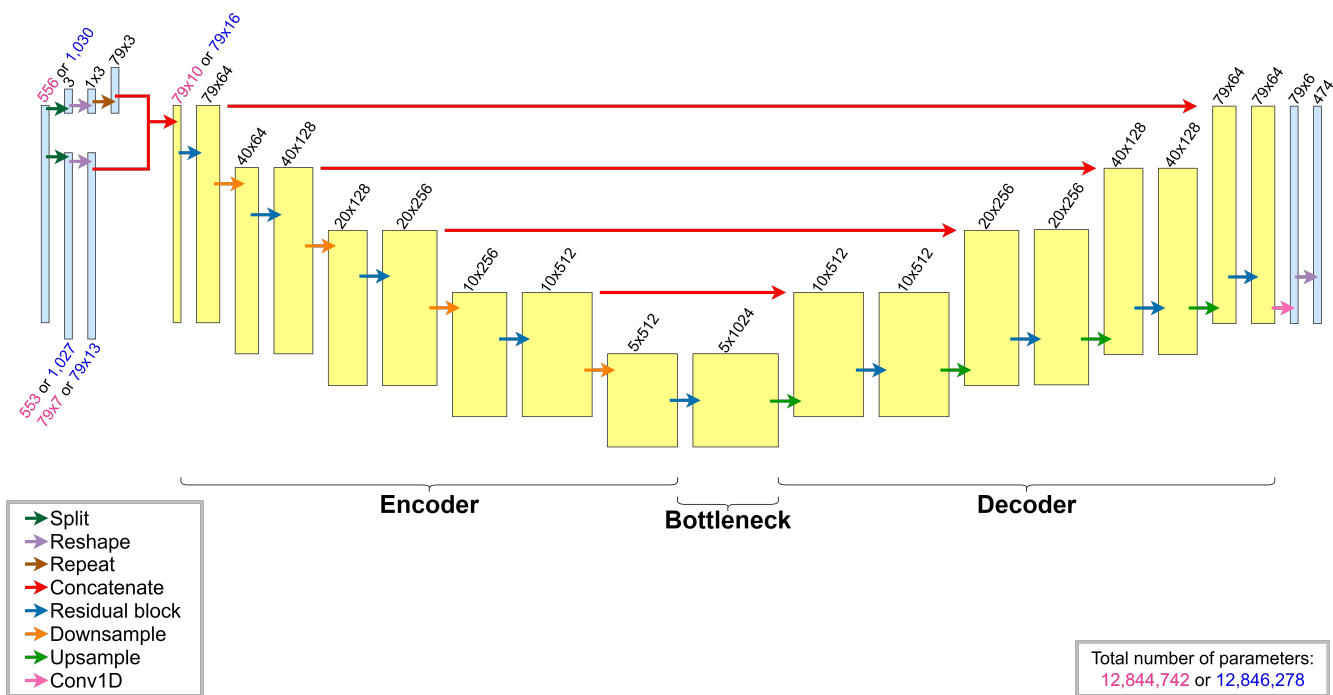


Figure S2. Diagram of the U-Net architecture. The blue and yellow boxes schematize the multi-channel features. The blue boxes correspond to the data formatting since the U-Net architecture —represented by the yellow boxes— works with 2D data whose dimensions correspond to the vertical levels times the number of variables. On the top (or sometimes the bottom) of each box is written the shape of the corresponding vector or tensor. The dimensions written in pink or blue at the start of the architecture are used to distinguish the size of data between the 1st learning (without laplacian) and the 2nd (with laplacians), respectively. The coloured arrows represent the different operations performed. The total number of parameters is indicated in pink for the 1st learning and in blue for the 2nd learning.

Table S2. Description of the U-Net architecture for the first training and the second. The pink and blue colours are used to distinguish differences in data shape between the 1st learning (without laplacian) and the 2nd (with laplacians), respectively. A residual block is composed by the succession of the following layers: Conv1D, BatchNormalization, ReLU, Conv1D, BatchNormalization, Add —to sum the input with the transformed output— and ReLU. A downsample layer corresponds to a MaxPooling1D. An upsample layer encompasses a Conv1DTranspose layer and a Concatenate layer which corresponds to the skip connection.

Step	Layer	Number of features	Number of filters (or channels)	Number of parameters 1 st learning	Number of parameters 2 nd learning
Input	Input	X' length	-	0	0
	Split	553 and 3	-	0	-
		1,027 and 3	-	-	0
	Lambda (reshape)	79	7	0	-
		79	13	-	0
		1	3	0	0
	Lambda (repeat)	79	3	0	0
	Concatenate	79	10	0	-
79		16	-	0	
Encoder	Residual block	79	64	15,808	17,344
	Downsample 1	40	64	0	0
	Residual block	40	128	83,840	83,840
	Downsample 2	20	128	0	0
	Residual block	20	256	233,216	233,216
	Downsample 3	10	256	0	0
	Residual block	10	512	1,318,400	1,318,400
	Downsample 4	5	512	0	0
Bottleneck	Residual block	5	1024	5,258,240	5,258,240
Decoder	Upsample 1	10	512	1,573,376	1,573,376
	Residual block	10	512	2,891,264	2,891,264
	Upsample 2	20	256	393,472	393,472
	Residual block	20	256	724,736	724,736
	Upsample 3	40	128	98,432	98,432
	Residual block	40	128	182,144	182,144
	Upsample 4	80	64	24,640	24,640
	Residual block	79	64	46,016	46,016
Output	Conv1D	79	6	1,158	1,158
	Lambda (reshape)	Y' length	-	0	0
Total number of parameters				12,844,742	12,846,278

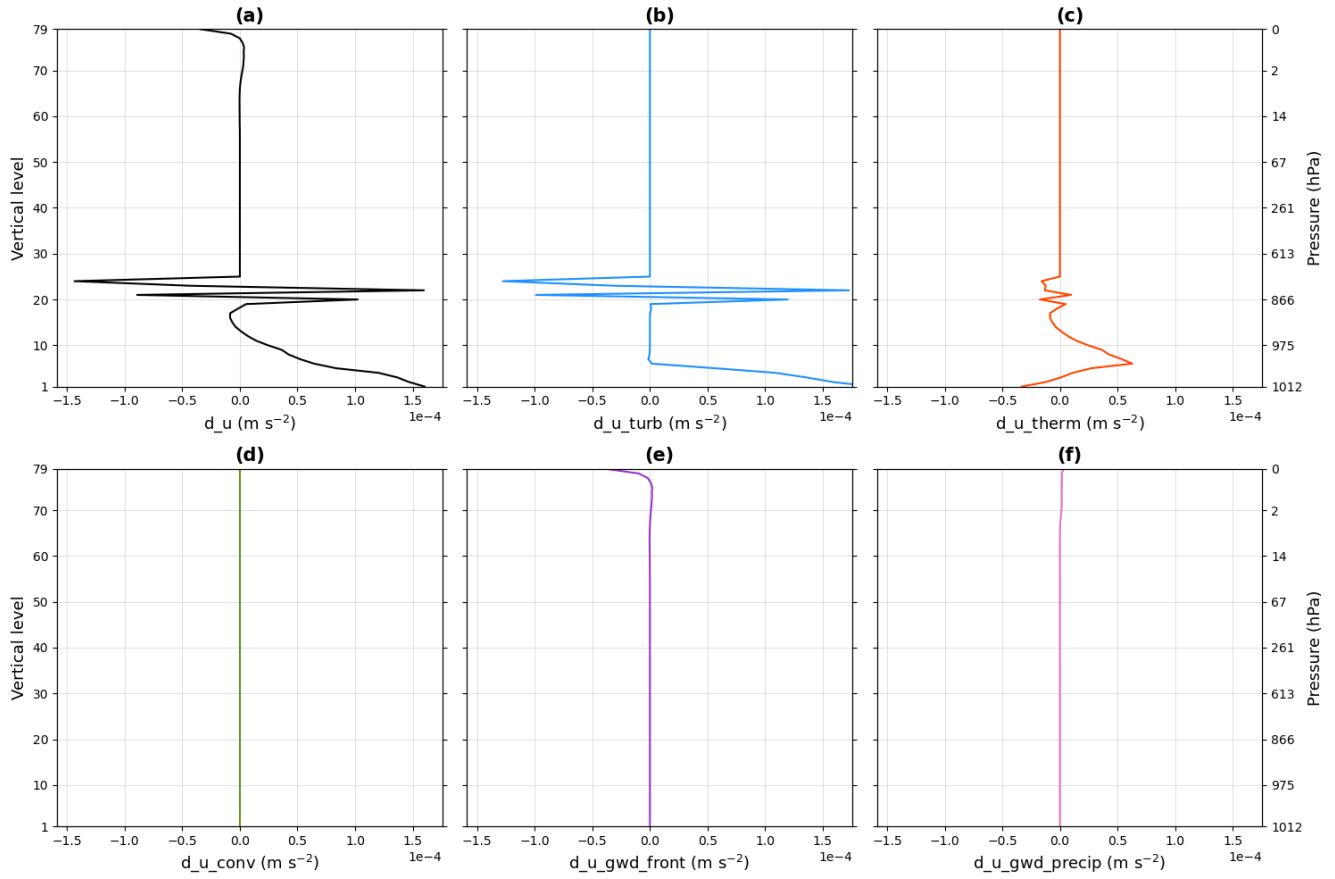


Figure S3. Vertical profile of the zonal wind tendency d_u (a) of the point A located in high latitudes for one time step, and vertical profiles of the physical processes involved in the decomposition of this tendency: turbulence (b), thermals (c), convection (d), gravity wave drag due to emission by fronts (e) and gravity wave drag due to emission by convective systems (f).

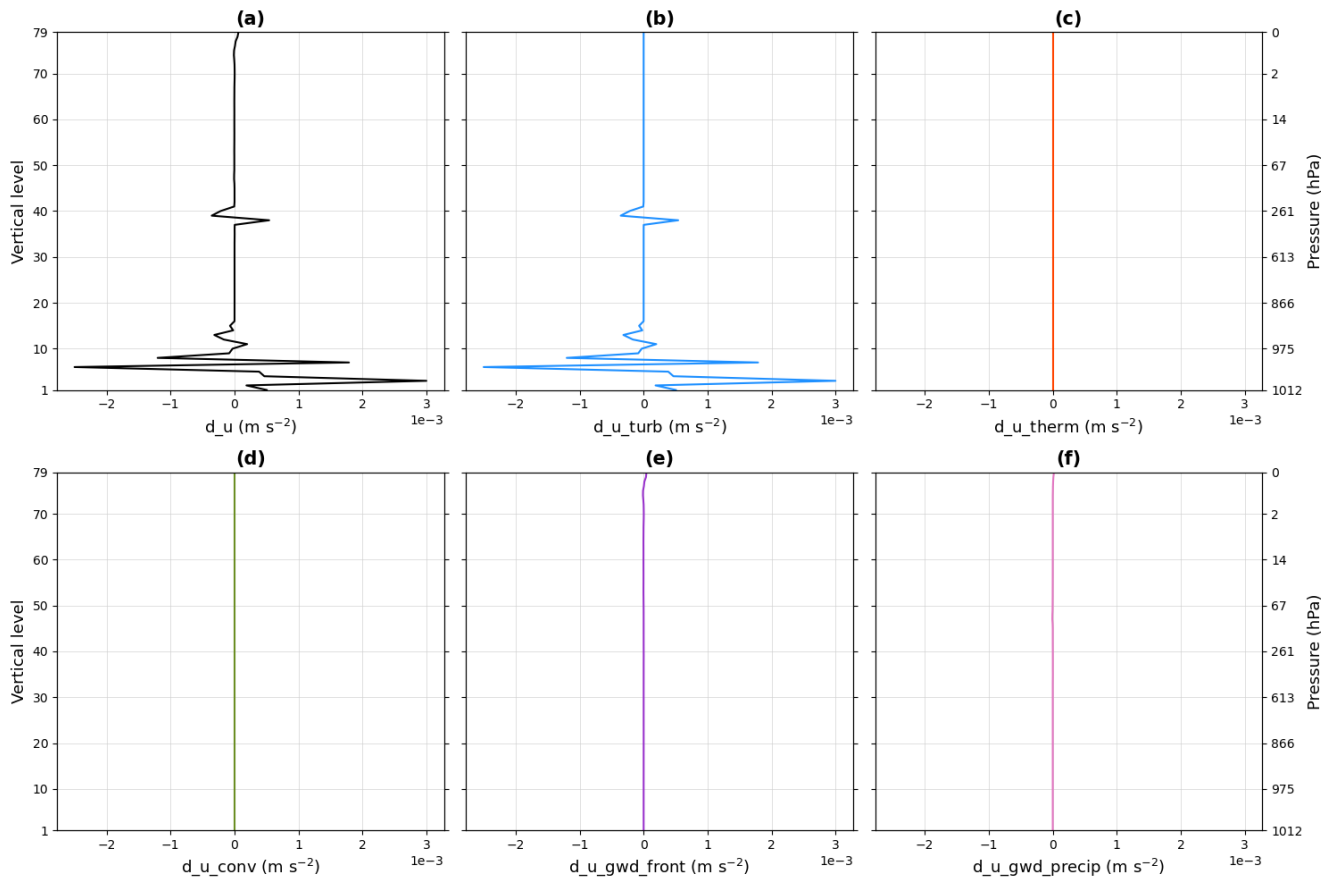


Figure S4. Same as Fig. S3 but for point B located in the subtropics.

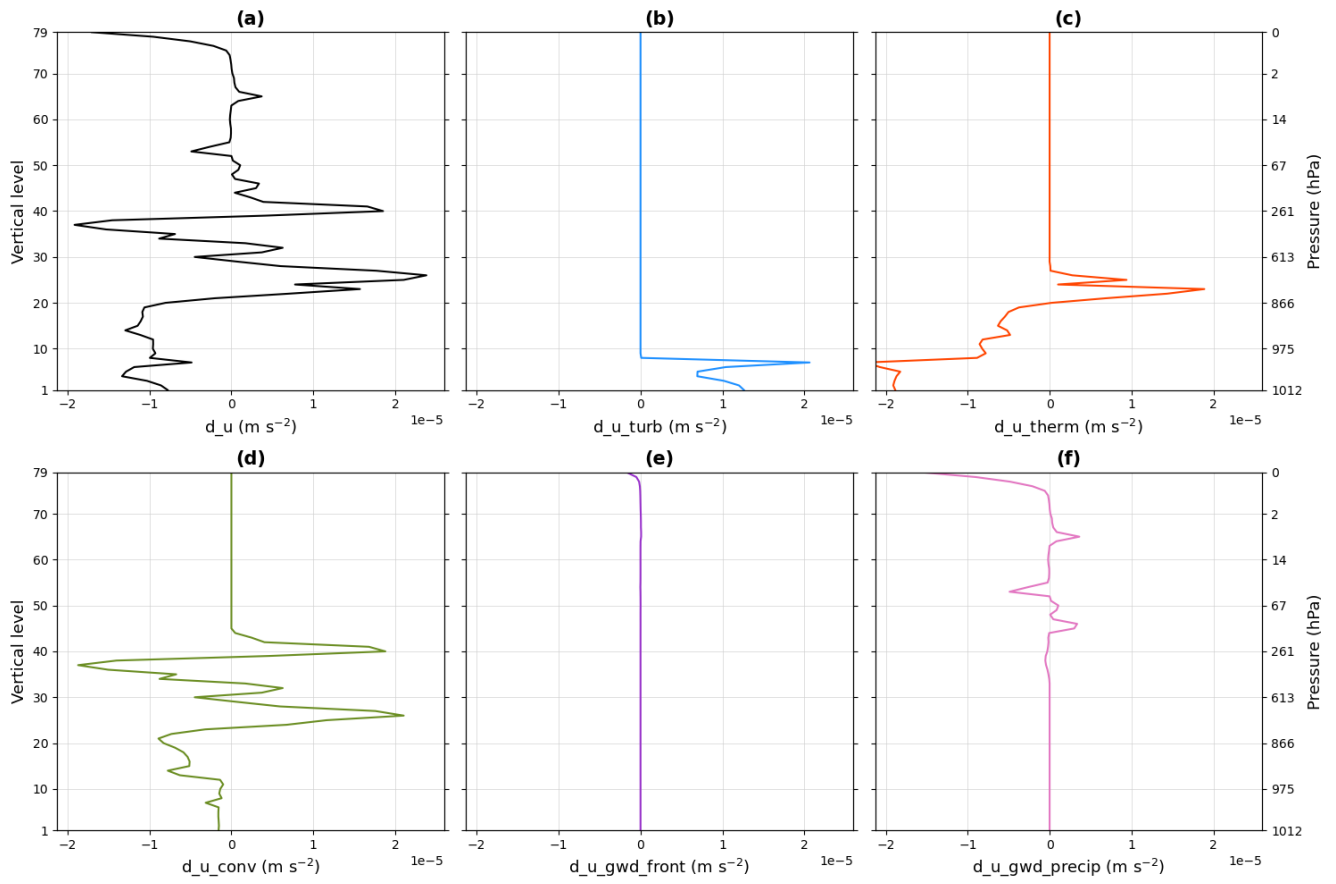


Figure S5. Same as Fig. S3 but for point C located near the equator.

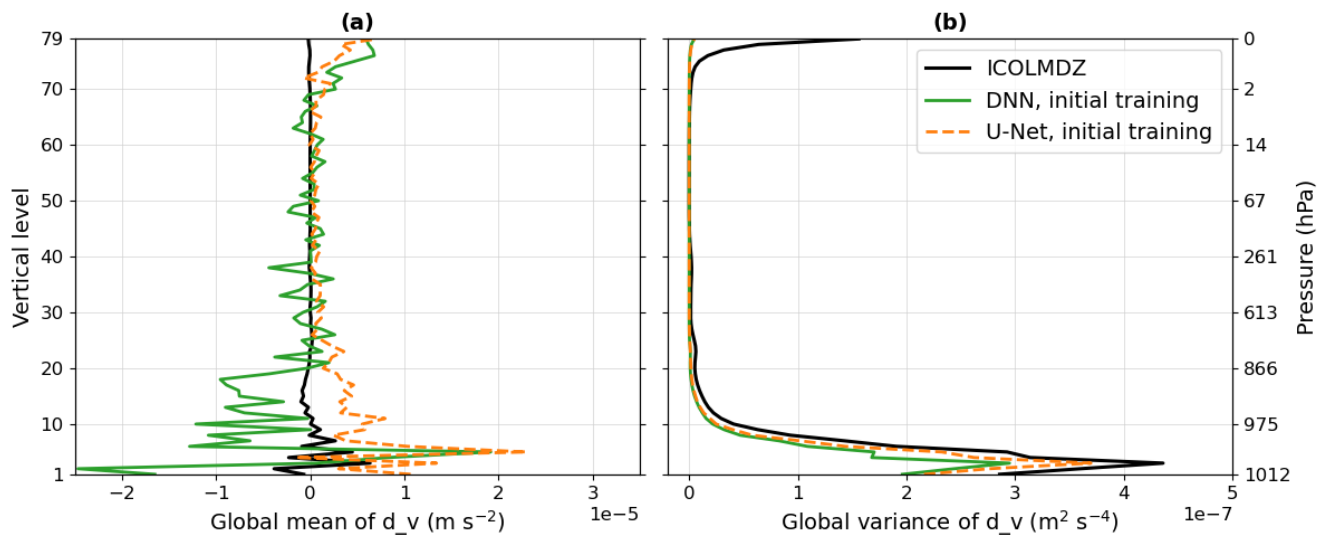


Figure S6. Same as Fig. 3 but for the meridional wind tendency d_v .

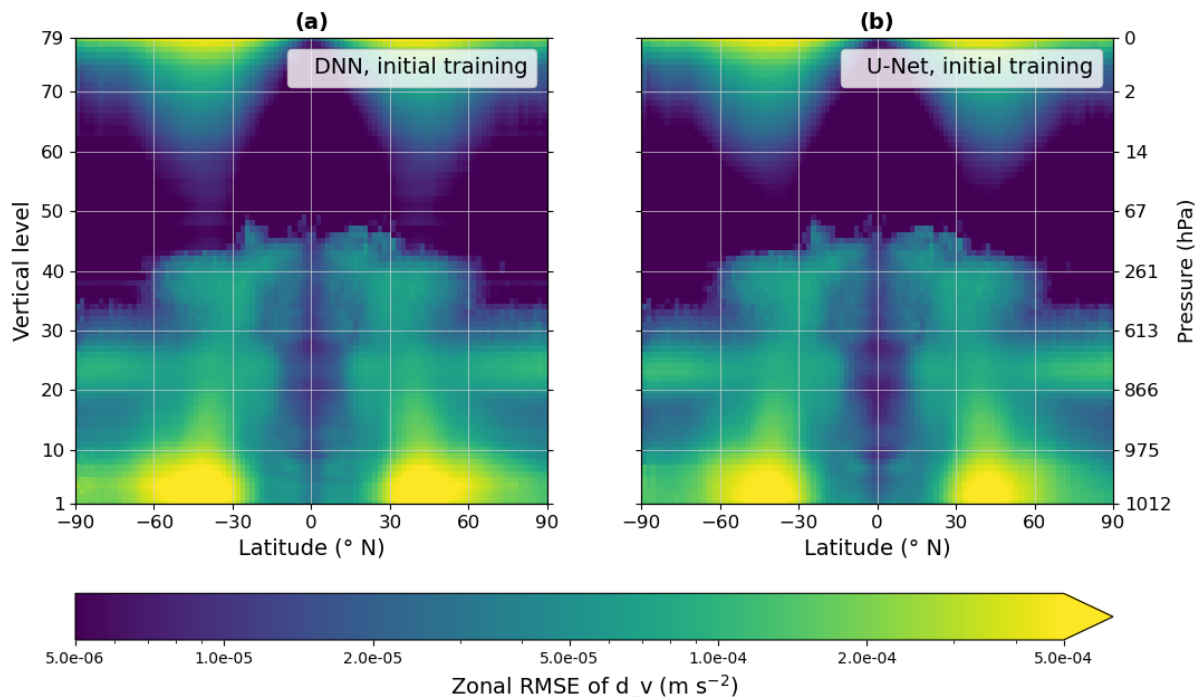


Figure S7. Same as Fig. 4 but for the meridional wind tendency d_v .

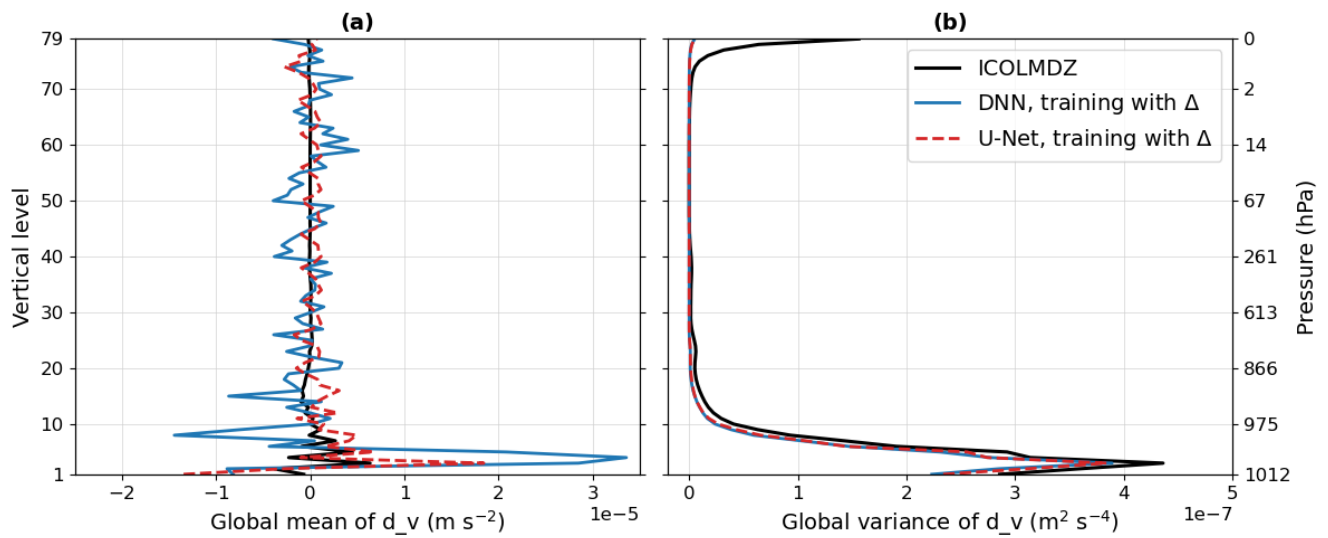


Figure S8. Same as Fig. 9 but for the meridional wind tendency d_v .

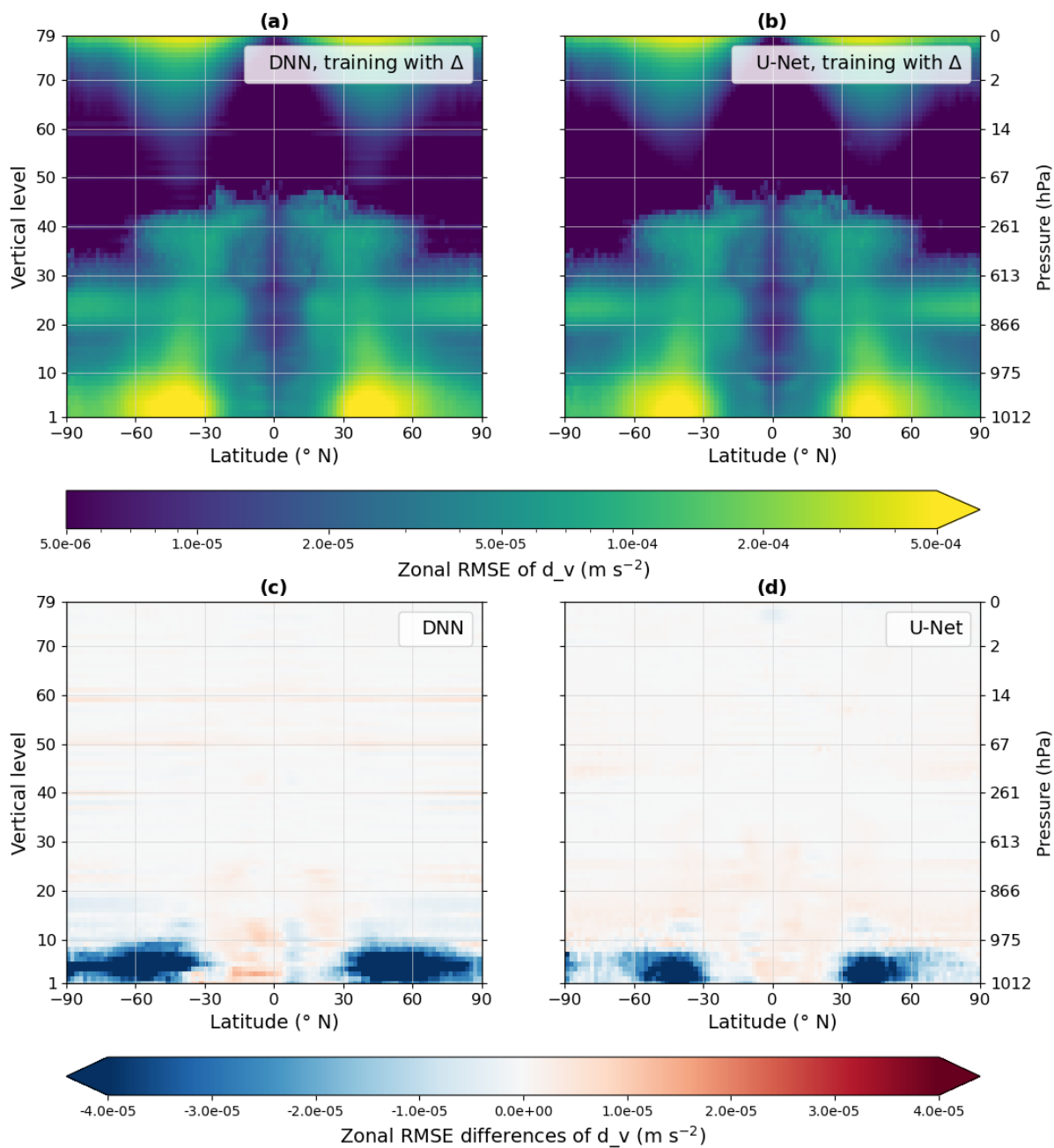


Figure S9. Same as Fig. 10 but for the meridional wind tendency d_v .

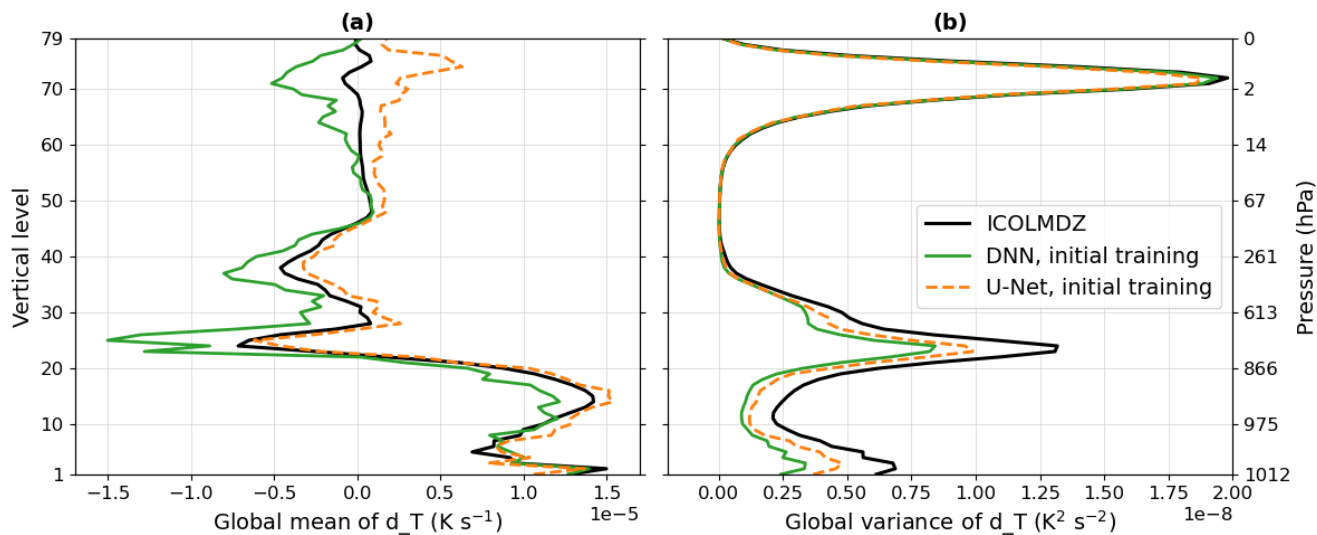


Figure S10. Same as Fig. 3 but for the temperature tendency d_T .

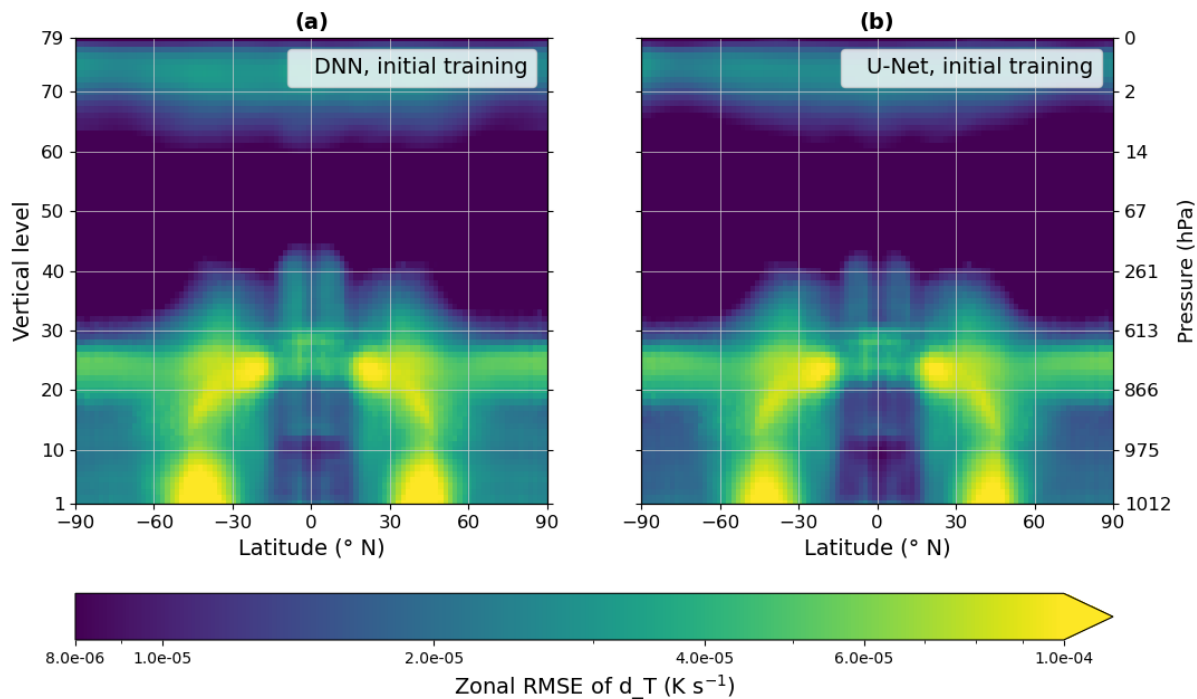


Figure S11. Same as Fig. 4 but for the temperature tendency d_T .

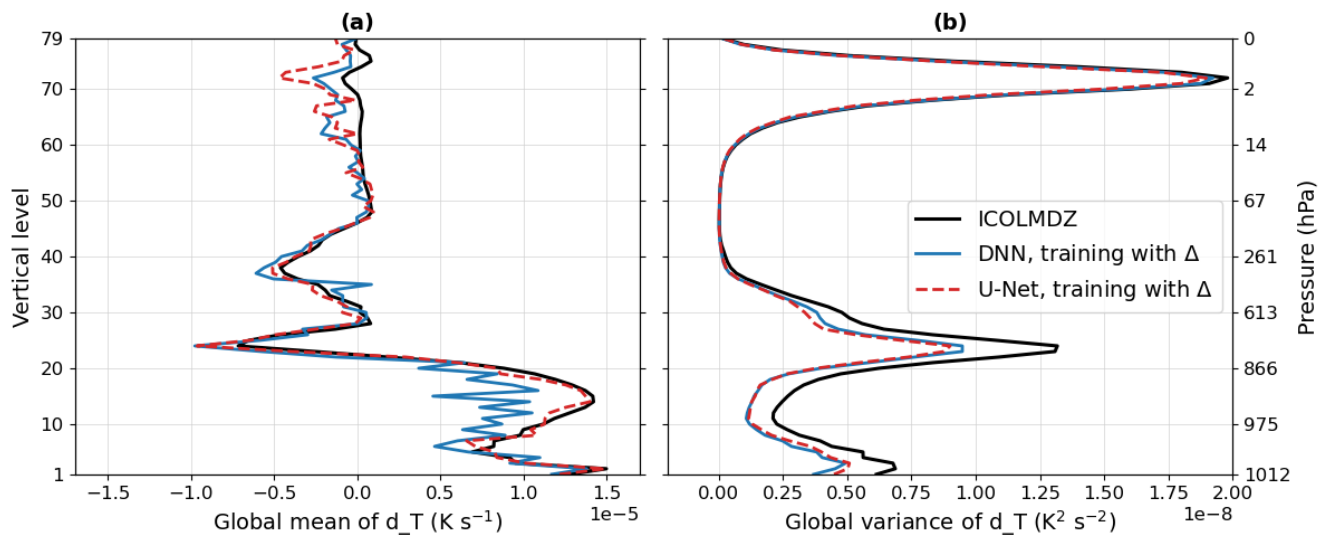


Figure S12. Same as Fig. 9 but for the temperature tendency d_T .

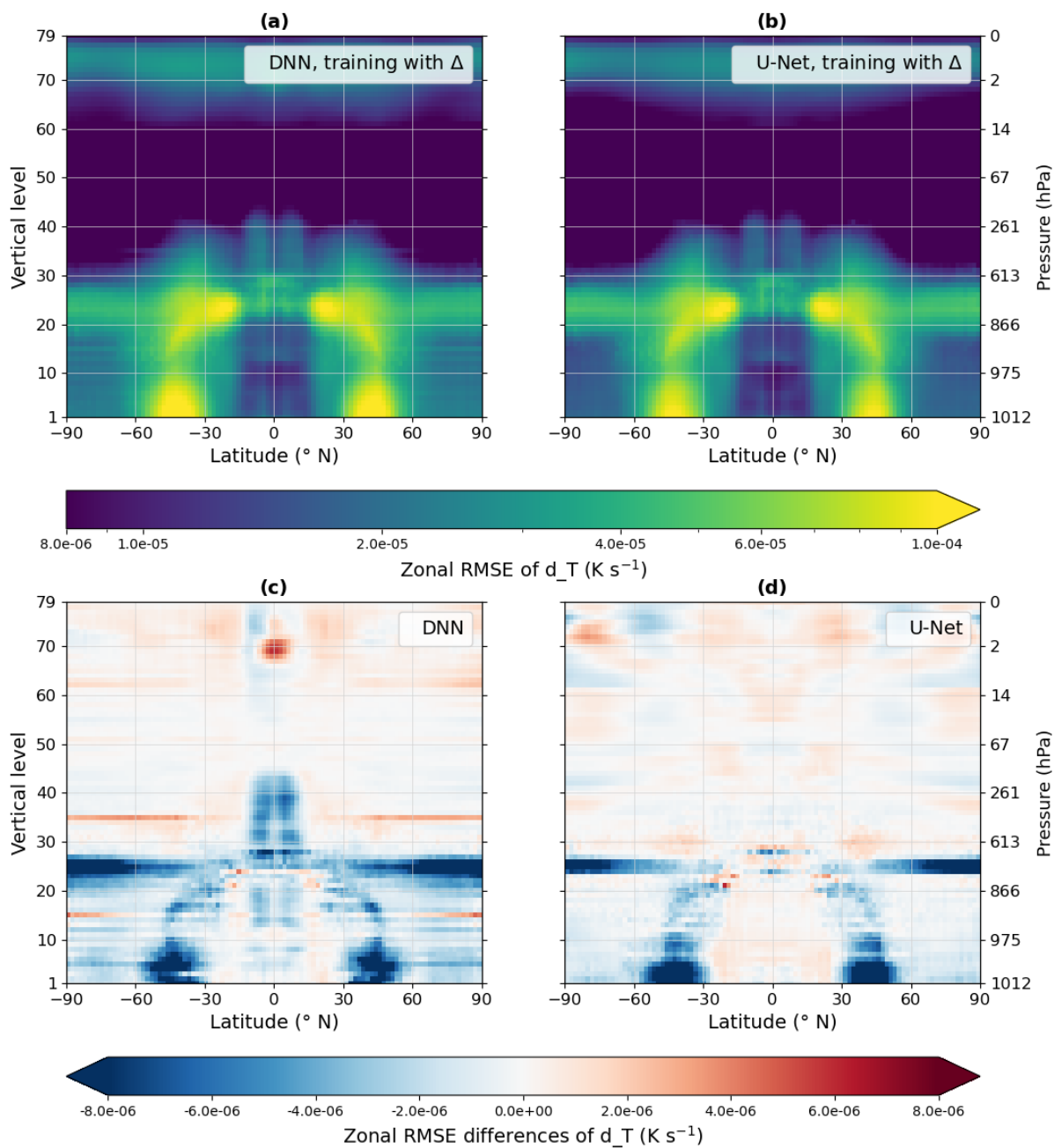


Figure S13. Same as Fig. 10 but for the temperature tendency d_T .

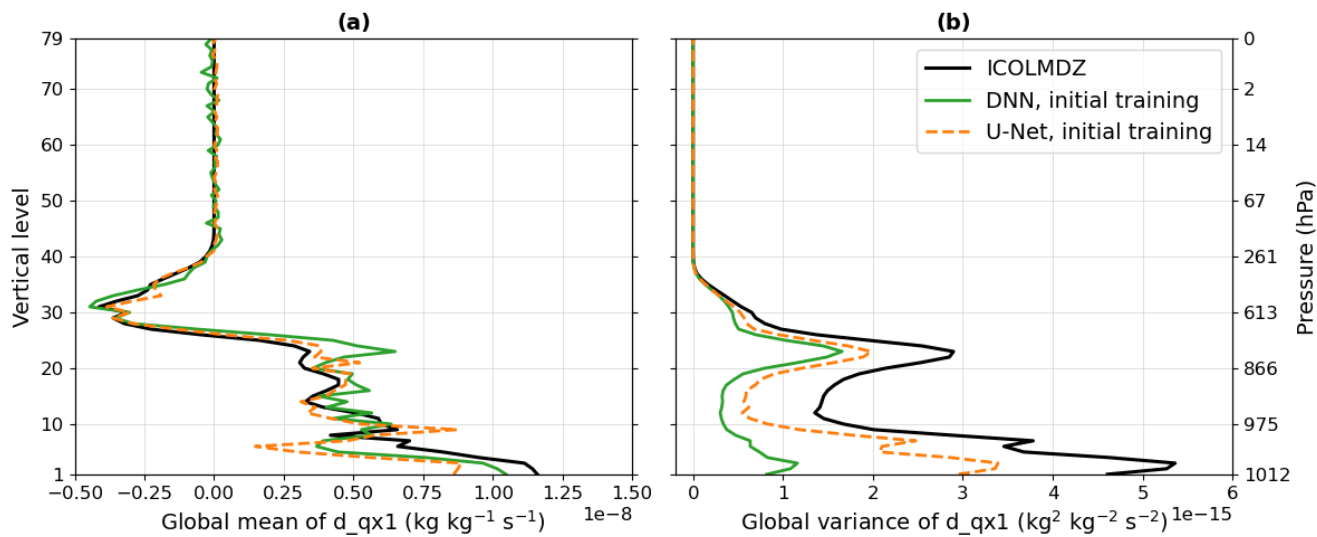


Figure S14. Same as Fig. 3 but for the humidity tendency d_{qx1} .

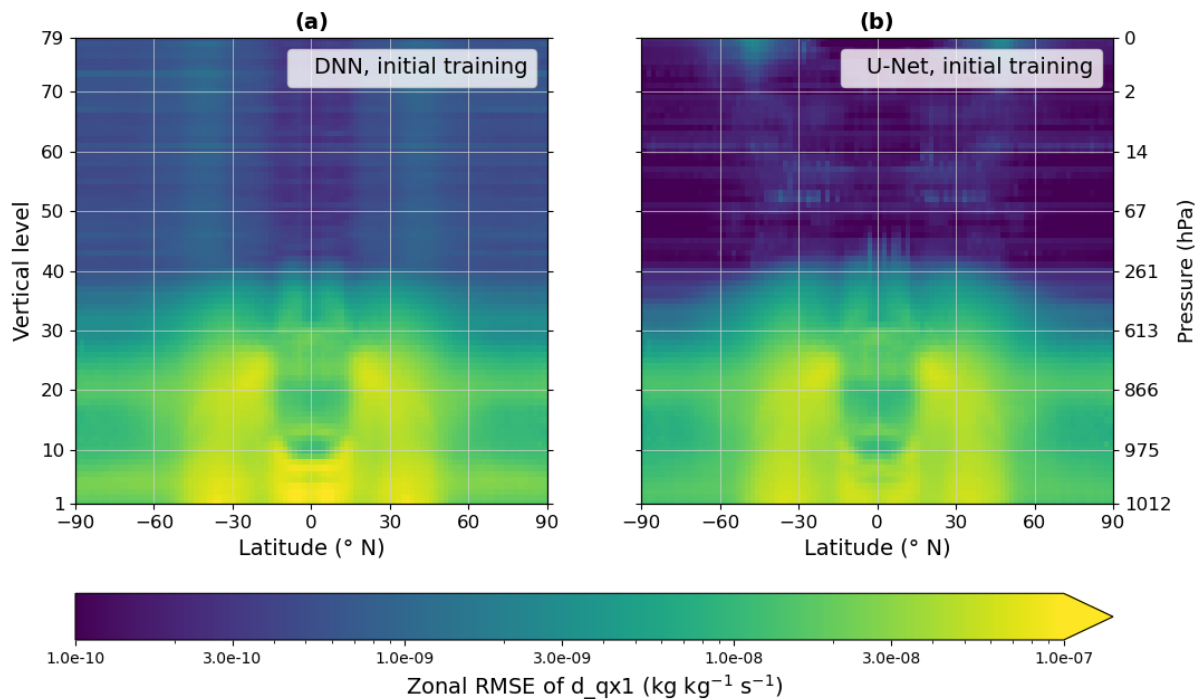


Figure S15. Same as Fig. 4 but for the humidity tendency d_{qx1} .

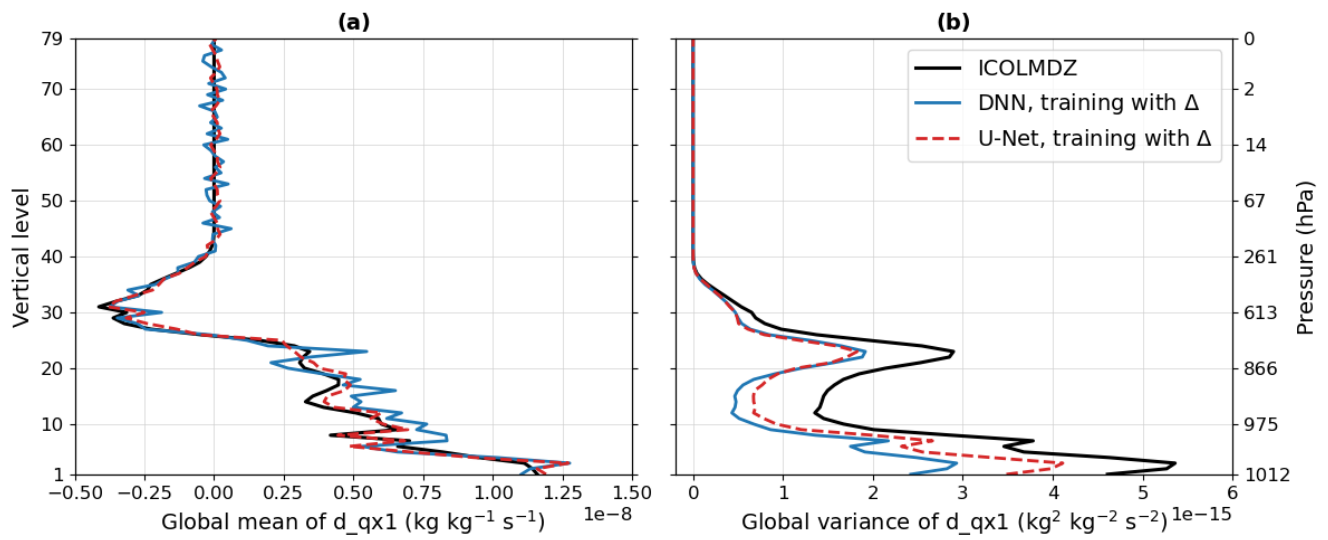


Figure S16. Same as Fig. 9 but for the humidity tendency d_{qx1} .

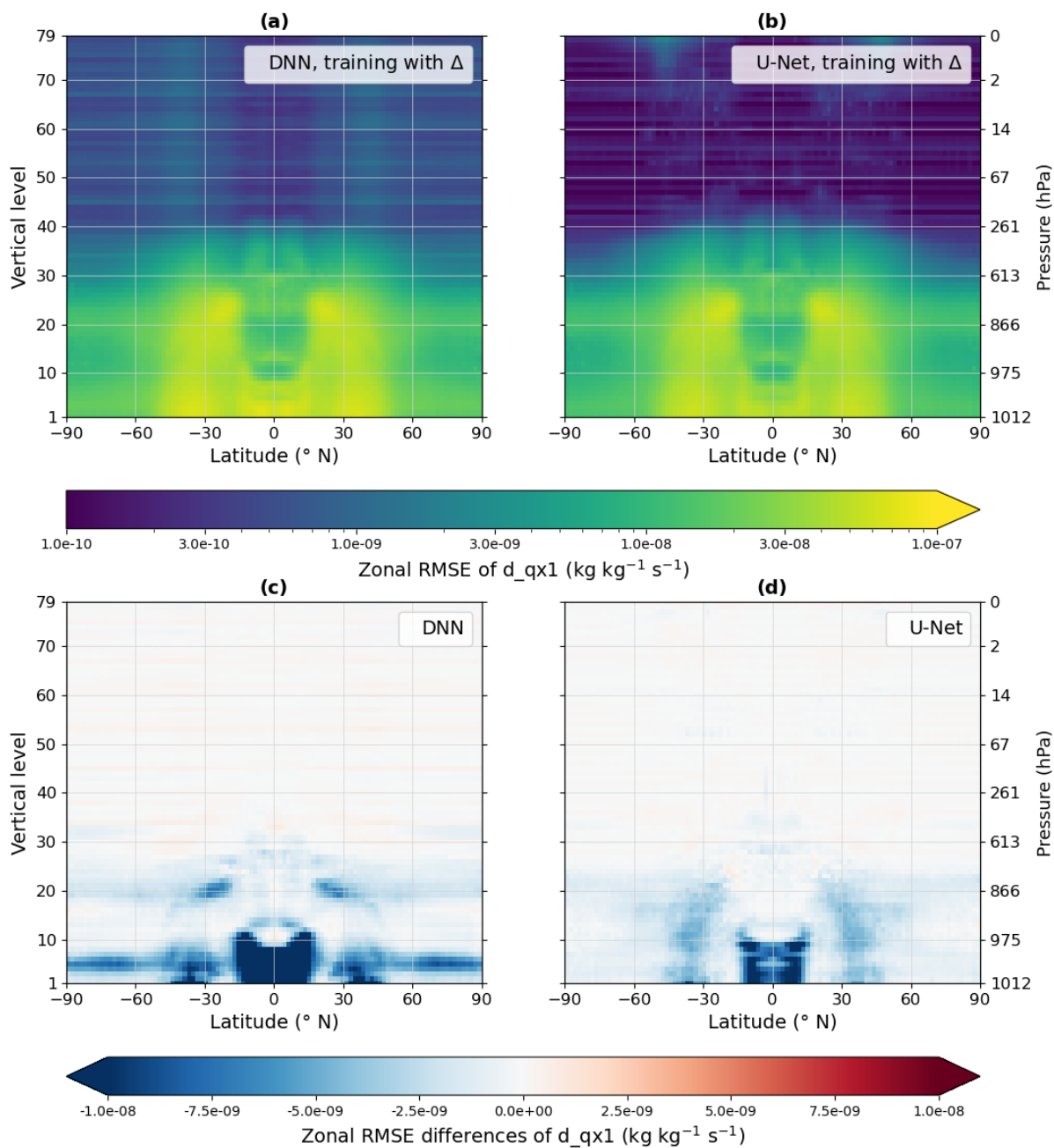


Figure S17. Same as Fig. 10 but for the humidity tendency d_{qx1} .

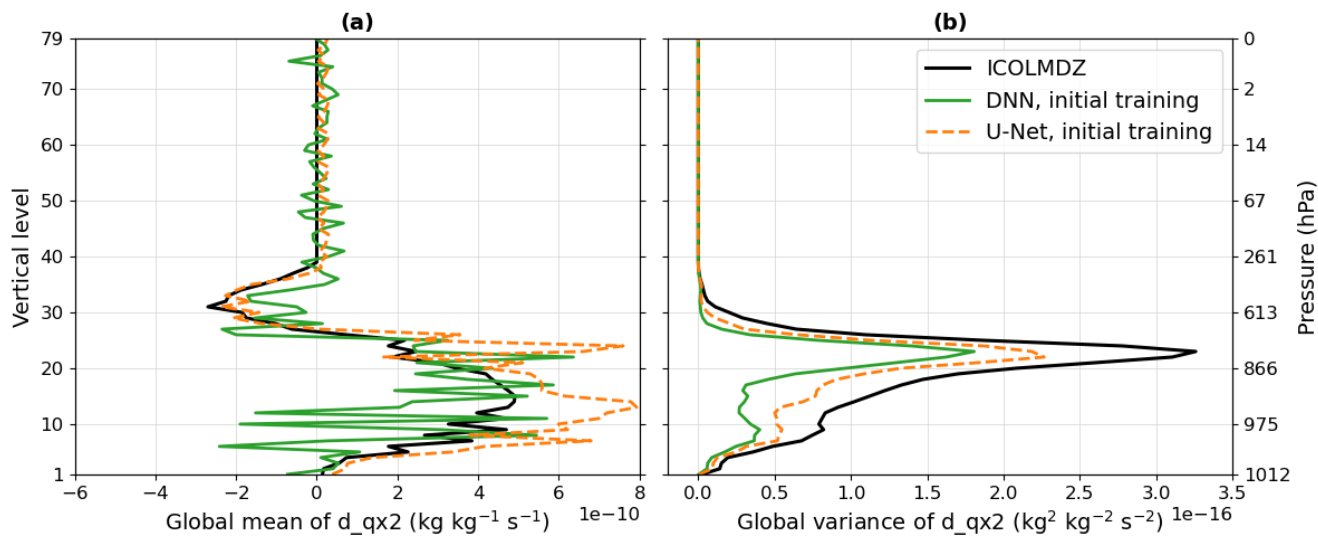


Figure S18. Same as Fig. 3 but for the liquid water tendency d_{qx2} .

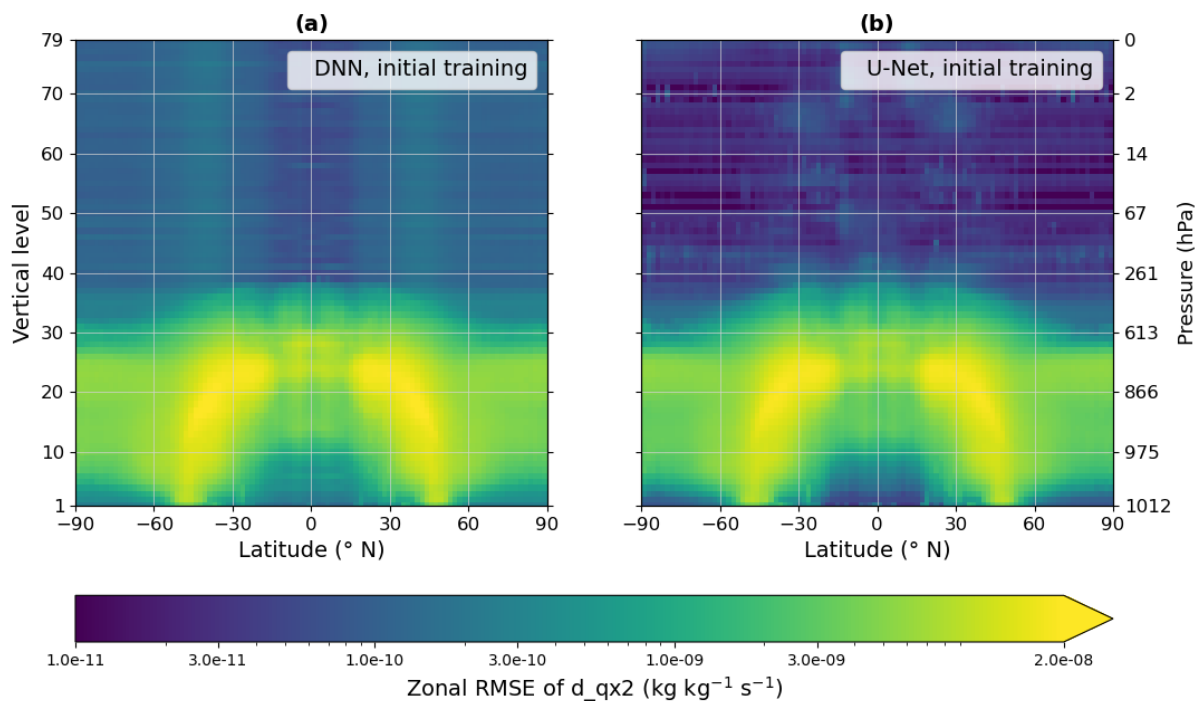


Figure S19. Same as Fig. 4 but for the liquid water tendency d_{qx2} .

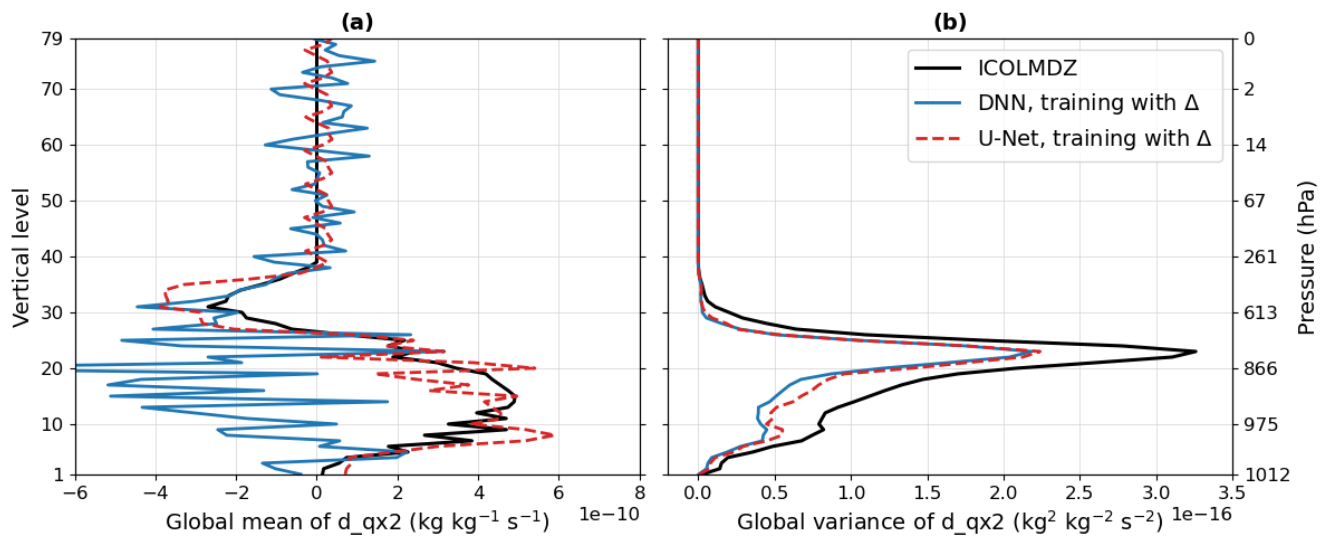


Figure S20. Same as Fig. 9 but for the liquid water tendency d_{qx2} .

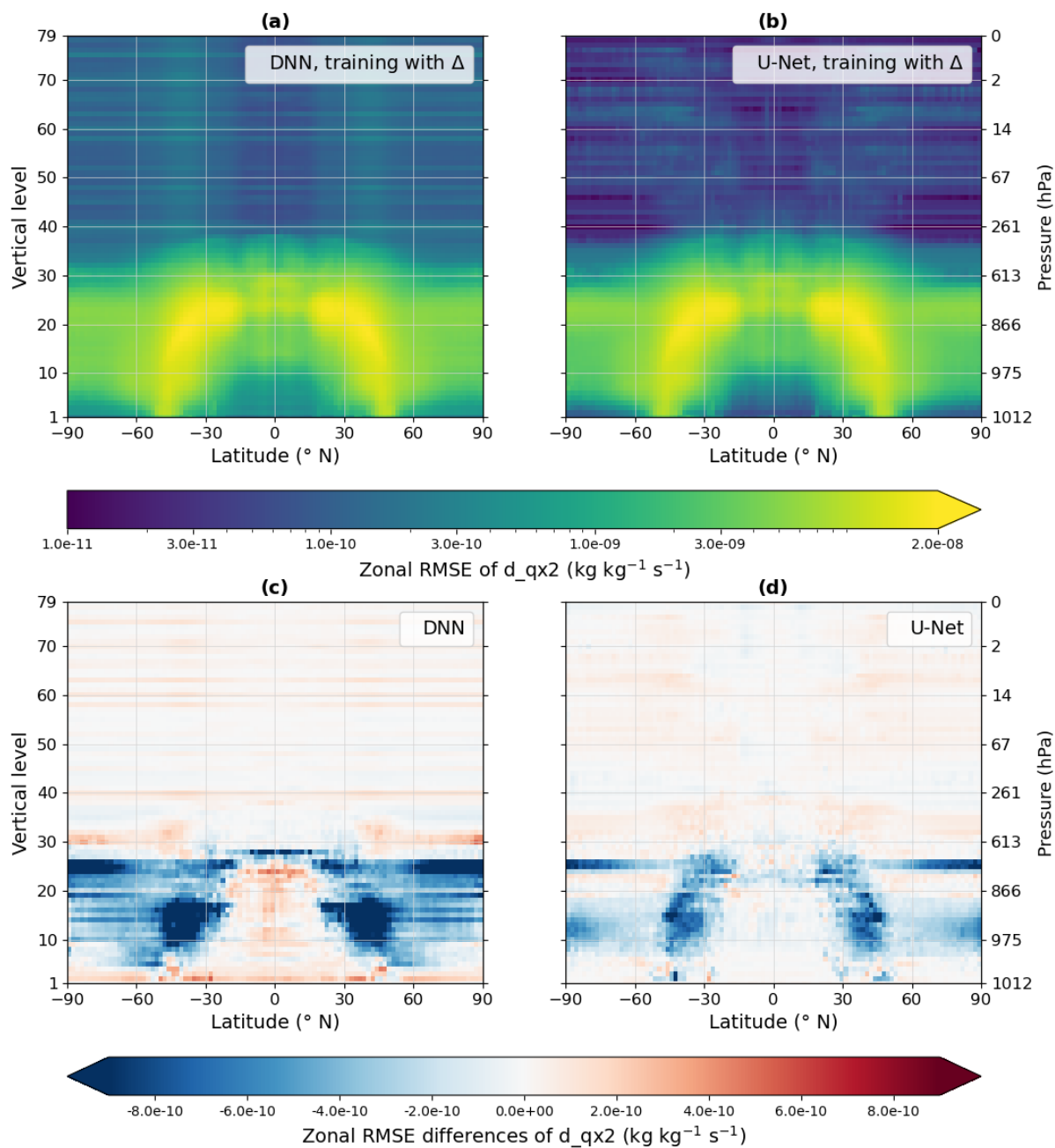


Figure S21. Same as Fig. 10 but for the liquid water tendency d_{qx2} .

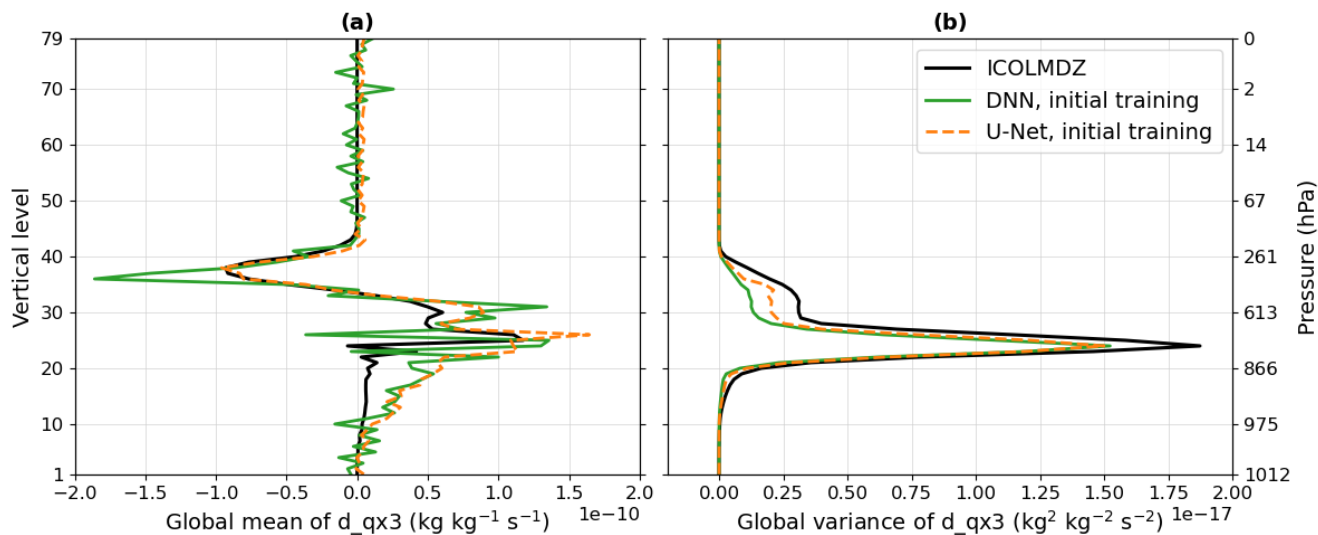


Figure S22. Same as Fig. 3 but for the solid water tendency d_{qx3} .

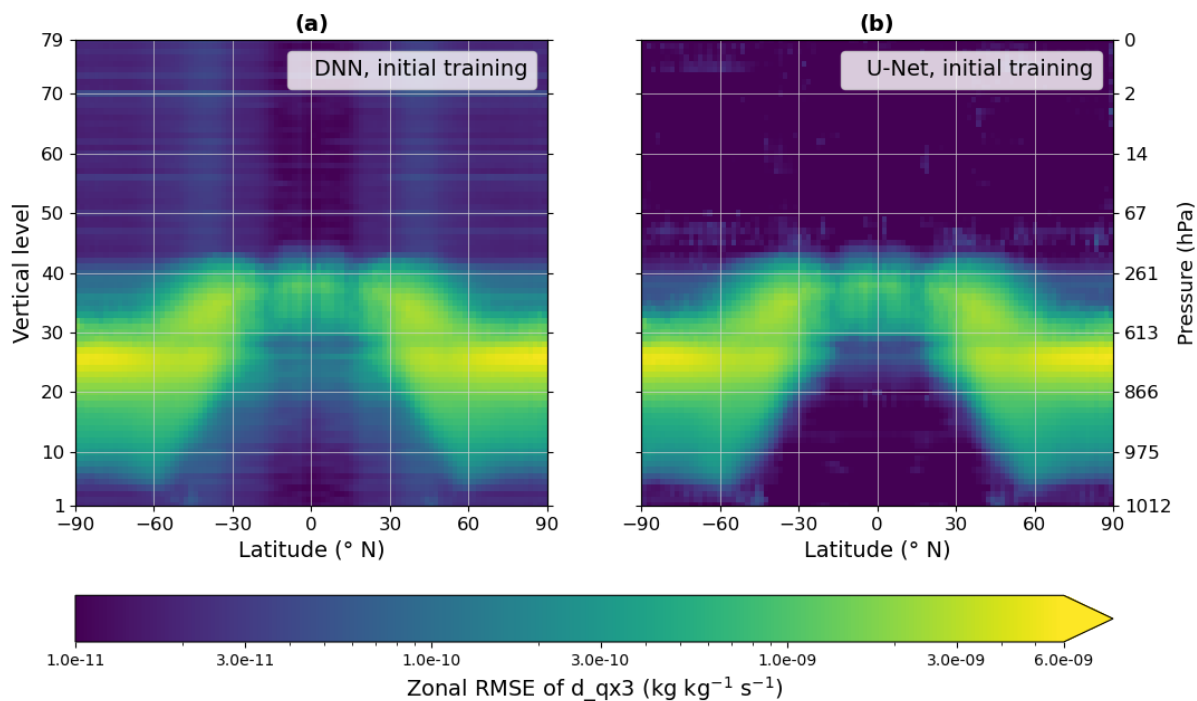


Figure S23. Same as Fig. 4 but for the solid water tendency d_{qx3} .

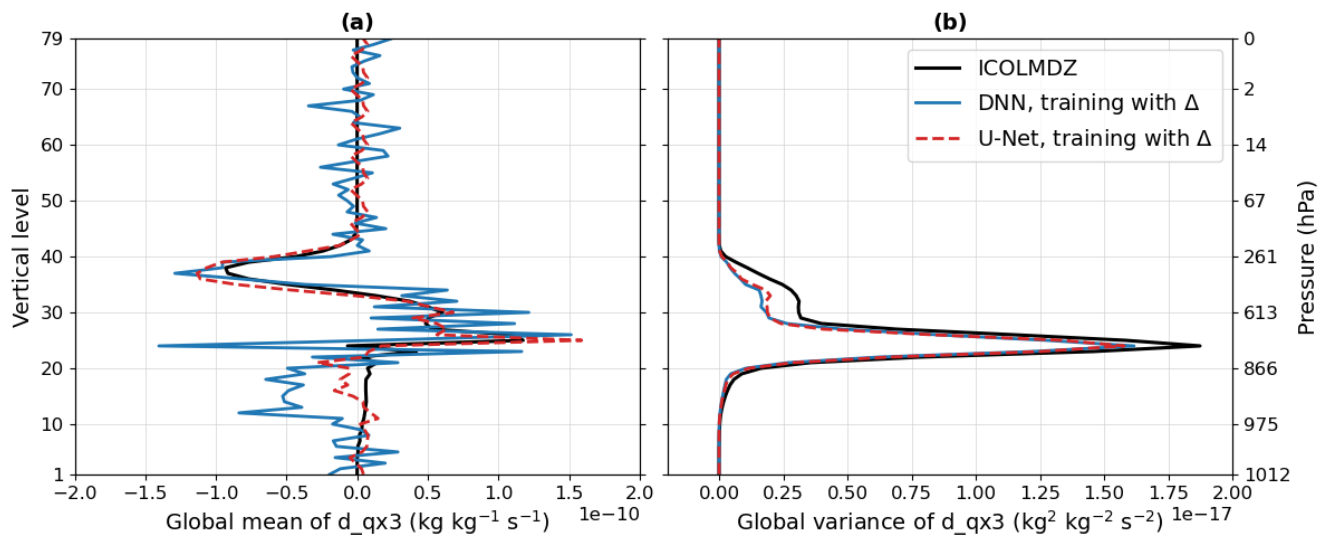


Figure S24. Same as Fig. 9 but for the solid water tendency d_{qx3} .

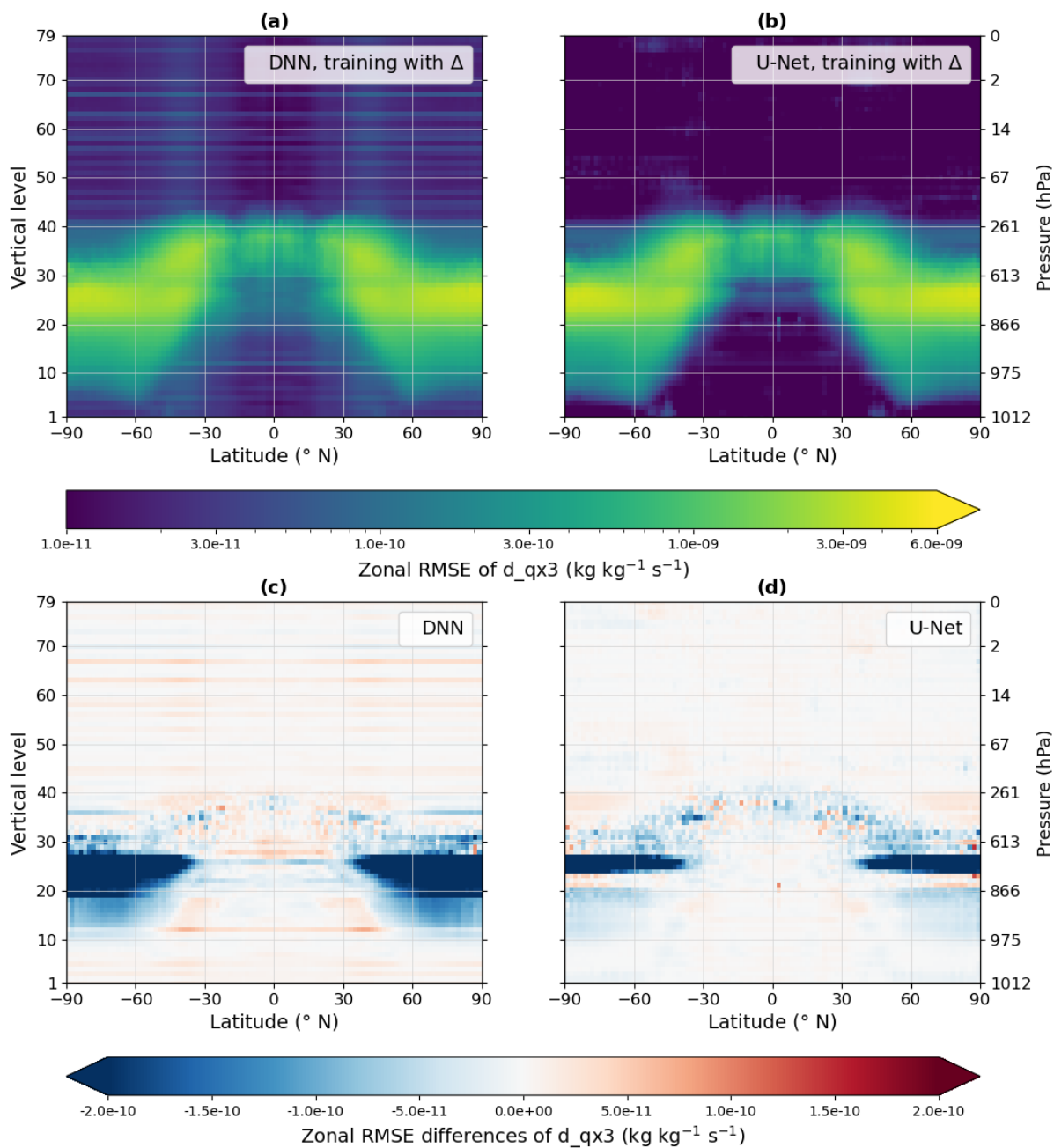


Figure S25. Same as Fig. 10 but for the solid water tendency d_{qx3} .